

Research Article

Multichannel Vestibular Prosthesis Employing Modulation of Pulse Rate and Current with Alignment Precompensation Elicits Improved VOR Performance in Monkeys

NATAN S. DAVIDOVICS^{1,2,3}, MEHDI A. RAHMAN^{1,2,3}, CHENKAI DAI^{2,3}, JOONGHO AHN^{2,3}, GENE Y. FRIDMAN^{2,3}, AND CHARLES C. DELLA SANTINA^{1,2,3}

¹*Department of Biomedical Engineering, Johns Hopkins University, Baltimore, USA*

²*Department of Otolaryngology–Head and Neck Surgery, Johns Hopkins University, Baltimore, USA*

³*Vestibular NeuroEngineering Laboratory, Johns Hopkins School of Medicine, Ross Bldg Rm 830, 720 Rutland Ave, Baltimore, MD 21205, USA*

Received: 21 March 2012; Accepted: 2 January 2013; Online publication: 26 January 2013

ABSTRACT

An implantable prosthesis that stimulates vestibular nerve branches to restore the sensation of head rotation and the three-dimensional (3D) vestibular ocular reflex (VOR) could benefit individuals disabled by bilateral loss of vestibular sensation. Our group has developed a vestibular prosthesis that partly restores normal function in animals by delivering biphasic current pulses via electrodes implanted in semicircular canals. Despite otherwise promising results, this approach has been limited by insufficient velocity of VOR response to head movements that should inhibit the implanted labyrinth and by misalignment between direction of head motion and prosthetically elicited VOR. We report that significantly larger VOR eye velocities in the inhibitory direction can be elicited by adapting a monkey to elevated baseline stimulation rate and current prior to stimulus modulation and then concurrently modulating (“co-modulating”) both rate and current below baseline levels to encode inhibitory angular head velocity. Co-modulation of pulse rate and current amplitude above baseline can also elicit larger VOR eye responses in the excitatory direction than do either pulse rate modulation or current modulation alone. Combining these stimulation strategies with a precompensatory 3D coor-

dinate transformation improves alignment and magnitude of evoked VOR eye responses. By demonstrating that a combination of co-modulation and precompensatory transformation strategies achieves a robust VOR response in all directions with significantly improved alignment in an animal model that closely resembles humans with vestibular loss, these findings provide a solid preclinical foundation for application of vestibular stimulation in humans.

Keywords: vestibular implant, vestibular prosthesis, rhesus, macaque, electrical stimulation, precompensation, co-modulation, neurostimulation

INTRODUCTION

Individuals with unilateral vestibular deficits are often able to compensate for their sensory loss via rehabilitation exercises and adaptation (Curthoys and Halmagyi 1995; Black et al. 1996). However, those with bilateral vestibular deficiency (BVD) due to ototoxic drug exposure, Ménière’s disease, meningitis, genetic defects, or other insults to the inner ear often suffer from degraded visual acuity during head movements, in addition to postural instability and chronic disequilibrium (Minor 1998; Rinne et al. 1998; Black et al. 2001, 2004; Mamoto et al. 2002). For these individuals, an implantable neuroelectronic prosthesis that measures three-dimensional (3D) head rotation

Correspondence to: Charles C. Della Santina · Vestibular NeuroEngineering Laboratory · Johns Hopkins School of Medicine · Ross Bldg Rm 830, 720 Rutland Ave, Baltimore, MD 21205, USA. Telephone: +1-410-5027909; fax: +1-410-6142439; email: charley.dellasantina@jhu.edu

and stimulates the vestibular nerve accordingly could significantly improve quality of life.

The ability to evoke directionally appropriate vestibular ocular reflex (VOR) eye movements in response to electrical stimulation of vestibular nerve branches was described in detail by Cohen and Suzuki (Cohen et al. 1964; Suzuki et al. 1964, 1969; Suzuki and Cohen 1964). This approach was later adapted to a single-channel head-mounted prosthesis prototype with a gyroscope that detected head rotation about one axis (Gong and Merfeld 2000; Lewis et al. 2001, 2002, 2010; Gong and Merfeld 2002; Merfeld et al. 2006, 2007; Gong et al. 2008). By delivering biphasic, symmetric, charge-balanced, rate-modulated pulses, the device generated partly compensatory eye movements for head rotations about the gyro's axis of rotational sensitivity. Wall, Guyot, and colleagues have applied a similar approach to single-channel vestibular nerve stimulation in humans (Wall et al. 2007; Guyot et al. 2011a, b, 2012), and Nie, Phillips, Rubinstein, and colleagues have recently applied analogous technology to monkeys and a human subject as part of an effort to develop a vestibular pacing device for treatment of Ménière's disease (Nie et al. 2011; Bierer et al. 2012; Rubinstein et al. 2012).

We extended this approach to a multichannel vestibular prosthesis (MVP) that senses 3D head rotation and encodes it via stimulation of all three ampullary nerves in the labyrinth, and we demonstrated its ability to partly restore the 3D VOR in both rodents and rhesus monkeys rendered vestibular deficient via bilateral intratympanic injection of gentamicin (Della Santina et al. 2005a, 2007; Fridman et al. 2010a; Dai et al. 2011b, c; Davidovics et al. 2011, 2012; Sun et al. 2011).

One of the central remaining challenges in prosthetic vestibular stimulation is the asymmetry of eye responses elicited by a unilateral implant. Eye movements tend to be larger for head movements moving the nose toward the implanted side (excitatory movements) than for head movements of equal speed in the opposite direction (inhibitory movements). This is likely the result of inherent asymmetries in the vestibular system. For example, rhesus monkey vestibular primary afferent fibers have a mean spontaneous firing rate of 107.4 ± 2.6 spikes/s (Sadeghi et al. 2007). Excitatory head movements can increase this firing rate up to ~ 500 spikes/s, but inhibitory head movements can only decrease the rate as low as 0 spikes/s. This results in significantly greater semicircular canal (SCC) sensitivity for head movements in the excitatory direction (and for excitatory electrical stimulation) than for the inhibitory direction (and for inhibitory down-modulation from baseline electrical stimulation). While bilateral implantation can achieve more symmetric VOR responses, clinical acceptance of

bilateral implantation for humans is unlikely for the first generation of the devices given risks and costs associated with bilateral surgery. Taking advantage of the vestibular system's exceptional ability to adapt to static imbalances in vestibular afferent input from the two labyrinths (Curthoys and Halmagyi 1995), one can elicit larger inhibitory eye movements with a unilateral implant by adapting a BVD animal to elevated unilateral baseline stimulation, which allows for increased dynamic range of stimulus down-modulation (Gong et al. 2008). However, this increase in inhibitory eye velocity comes at the cost of reduced excitatory eye velocity in response to stimulus up-modulation (Lewis et al. 2010).

While pulse rate modulation (aka pulse frequency modulation) is the most obvious choice for encoding head velocity in the vestibular prosthesis because it is most similar to the spike rate code apparently used by afferents in the normal labyrinth, alternate strategies may yield larger eye responses. We compared VOR eye velocities in response to pulse rate modulation, current modulation (aka pulse amplitude modulation), and simultaneous co-modulation of both rate and current. We hypothesized that current modulation alone would elicit eye response velocities similar to those elicited by rate modulation alone, but with greater misalignment. We also hypothesized that co-modulation would elicit larger eye response velocities than those elicited by either rate or current modulation alone, which would be particularly desirable in the case of diminished stimulus up-modulation range when modulating above an elevated baseline.

Another central problem in vestibular stimulation is cross talk between stimulating electrodes, which results in eye movement responses that are misaligned with their intended axes of rotation (Della Santina et al. 2005a, 2007; Fridman et al. 2010a; Davidovics et al. 2011). Prior work in chinchillas has resulted in coding strategies that successfully address this problem using an alignment precompensation strategy (Fridman et al. 2010a). For example, if stimulation intended to excite the horizontal ampullary nerve spuriously excited the anterior and posterior ampullary nerves, resulting in misaligned VOR response, deleterious effects of this cross talk could be minimized by effectively delivering inhibitory stimuli to the unintended nerve branches while simultaneously exciting the horizontal nerve.

Noting the differences in temporal bone anatomy and size between chinchillas and chronically disabled human subjects for whom the MVP is being developed, we sought to extend our studies from chinchilla to rhesus monkeys, which have temporal bone anatomy very similar to that of humans. Because the separation between different vestibular nerve branches in the rhesus labyrinth is ~ 1.5 – 1.7 times

greater in rhesus than in chinchillas (Ramprashad et al. 1984), we hypothesized that rhesus monkeys would exhibit findings at least as close to normal as those we have observed in chinchillas. Furthermore, even though elevated baseline stimulation with co-modulation and alignment precompensation strategies have both been shown to improve eye responses when employed separately, we sought to determine the eye response effects of simultaneously adapting the animal to elevated baseline stimulation and delivering co-modulated stimuli with alignment precompensation. These experiments have the potential to provide the basis for vestibular stimulation encoding strategies in future human clinical trials.

MATERIALS AND METHODS

Surgery

Two rhesus monkeys (5–7 kg; one female, one male) were used for all experiments, which were performed in accordance with a protocol approved by the Johns Hopkins Animal Care and Use Committee, which is accredited by the Association for the Assessment and Accreditation of Laboratory Animal Care International and consistent with European Community Directive 86/609/EEC. Our methods for surgical implantation of a head-fixation mechanism and scleral coils for magnetic search coil recording of 3D eye movements in primates have been described previously (Minor et al. 1999; Dai et al. 2011c). With the animal under general inhalational anesthesia (1.5–5 % isoflurane), a light poly-ether-ether-ketone head cap was affixed to the skull under sterile conditions using titanium bone screws and poly-methyl methacrylate. Two search coils were fashioned from polytetrafluoroethylene-coated steel wire (Cooner Wire, Chatsworth, CA) and sutured to the sclera of one eye, with one around the iris and the other approximately orthogonal to the first. Wires were tightly twisted to reduce inductive artifacts and then run to connectors within the head cap. Animals were maintained under general anesthesia for surgery and treated with analgesics and antibiotics for 72 h perioperatively.

Prior to any intervention of either labyrinth, normal VOR performance was characterized during whole-body rotations in darkness for 50 °/s peak velocity sinusoids at 0.05, 0.1, 0.2, 0.5, 1, 2, and 5 Hz and for acceleration steps of 1,000 °/s² to a plateau velocity of 150 °/s using the eye movement measurement methods described below (Dai et al. 2011c). Gains for rotational frequencies 0.5–5 Hz were close to one for all three SCC axes tested.

After characterization of an animal's normal VOR performance, a separate surgery was performed to implant an electrode array in the left labyrinth via a

transmastoid approach similar to that used for cochlear implantation or labyrinthectomy (Dai et al. 2011c). Under sterile conditions, a cortical mastoidectomy was performed. The junction of the ampullae of the superior and horizontal SCCs was identified, and two small holes were made there, keeping a thin strut of bone intact between the two to serve as a stop when inserting the forked electrode array. An opening was also made in the thin segment of the posterior SCC near its junction with the ampulla, into which the single-tine electrode array was inserted. Pieces of fascia were tucked around each array, and a small amount of dental cement (Protemp ESPE, 3M Corp) was optionally used to stabilize the electrode leads, which were run under periosteum to the head cap.

After unilateral electrode array implantation, ototoxic doses of gentamicin were delivered bilaterally via intratympanic injection using a regimen similar to that used in humans (Carey et al. 2002), except that the animal was maintained under general inhalational anesthesia (1.5–5 % isoflurane) for 30 min with the treated ear up to help ensure adequate diffusion of drug across the round window and into the inner ear (Dai et al. 2011a; b). For each treatment, ~0.5 mL of 26.7 mg/mL buffered gentamicin solution was injected through the eardrum into the middle ear. Delivered via this route, gentamicin accumulates in hair cells and ultimately ablates labyrinthine mechanosensitivity by destroying type I hair cells and by denuding type II hair cells of their stereocilia (Hirvonen et al. 2005; Lyford-Pike et al. 2007). Notably, about half of human patients treated with intratympanic gentamicin for Ménière's disease require more than one injection to achieve the desired drop in labyrinthine function (Nguyen et al. 2009). A similar effect was noted in the present study, so treatments were repeated every 3 weeks until VOR responses to head rotation toward the treated ear reduced to <10 % of normal gain, which required two or three injections per ear in each case (Dai et al. 2011b).

Eye movement recording

The eye coil system used to measure 3D angular eye position has been described in detail previously (Robinson 1963; Migliaccio et al. 2004). The monkey was seated in a plastic chair with its head restrained by the skull cap. Three pairs of field coils were rigidly attached to the superstructure, generating three fields orthogonal to each other and initially aligned with the X (nasooccipital, +nasal), Y (interaural, +left), and Z (superoinferior, +superior) stereotactic head coordinate axes and oscillating at 79.4, 52.6, and 40.0 kHz, respectively.

To facilitate real-time interpretation of eye movement recording signals, we reoriented the animal's head within the coil frame to better align the SCC axes with the coil frame. From the initial stereotactic alignment position, the animal's head was reoriented 15° (animal 1) or 19° (animal 2) nose down about the interaural axis to bring the mean horizontal SCC plane into the coil frame *XY* plane. (The mean horizontal SCC plane was determined individually for each animal individually from $0.234 \times 0.234 \times 0.5$ -mm voxel computed tomographic scans using techniques previously described to measure a best fit plane and relate it to stereotactic landmarks (Della Santina et al. 2005b). With the head in this orientation, the three frequency signals induced across each scleral coil were demodulated to produce three voltages proportional to the angles between the coil and each magnetic field and then analyzed using 3D rotational kinematic methods (Straumann 1995). All signals transducing motion of the head or the eye were passed through eight-pole Butterworth anti-aliasing filters with a corner frequency of 100 Hz prior to sampling at 200 Hz. Coil misalignment was corrected using an algorithm that calculated the instantaneous rotation of the coil pair with reference to its orientation when the eye was in a reference position (Tweed and Vilis 1990). Angular rotations were expressed as rotation vectors with roll, pitch, and yaw coordinates, and angular velocity vectors of the eye with respect to the head were calculated from the corresponding rotation vectors (Hepp 1990; Haslwanter 1995; Migliaccio and Todd 1999). Angular position resolution of the coil system was 0.2° (tested over the angular range of $\pm 25^\circ$ combined yaw, pitch, and roll positions), and angular velocity noise was $\sim 2.5^\circ/\text{s}$ peak.

Stimulation paradigm

Electrical stimulation of the vestibular nerves was delivered by a Johns Hopkins model MVP2 multi-channel vestibular prosthesis (Chiang et al. 2011). Rotational head velocity about each of three SCC axes was encoded by modulating pulse frequency and/or current amplitude of symmetric, charge-balanced, cathodic-first (at the SCC electrode) 150 μs /phase biphasic current pulses, using a head velocity to pulse rate mapping strategy that has been described in detail previously (Della Santina et al. 2007). The MVP2's circuitry was located within the animal's head cap and connected to the implanted electrode array via a percutaneous connector. This arrangement ensured rigid coupling between the MVP2's motion sensor and the skull while allowing us to replace or update the circuitry without explanting the electrode array. During an experiment, we communicated with the devices via a wireless (Bluetooth®) command

interface (to set stimulus parameters and initiate stimulation) and a buffered, wired analog interface (via which the MVP2 can report pulse rates on each channel and convey a synchronization signal to the eye movement recording system). Prior to initiation of physiologic experiments, calibration experiments were performed (using sense resistors in series with the electrodes and an oscilloscope with isolated differential amplifier inputs) to ensure that the MVP2 faithfully delivered stimuli with the timing and current commanded.

To ensure that recorded responses were due solely to prosthetic input, the head and body were kept stationary during measurements of the prosthetically evoked VOR eye movements, and the MVP2's gyroscopic signals were replaced with analog signals representing head rotation delivered under computer control in a dark room.

At the beginning of each experiment, the range of useful current amplitudes was determined for each SCC electrode by slowly increasing the current while 200-pps pulse trains of 75-ms duration were periodically delivered. Threshold current was determined to be the current amplitude that elicited an eye movement of $\sim 10^\circ/\text{s}$, and maximum current was determined to be just below the current that elicited visible facial muscle responses.

All stimulus pulse trains were 100-ms transient steps in pulse rate and/or current amplitude. These types of transient stimuli are the theoretical equivalent to head impulse movements experienced during typical "head thrusts" ($\sim 1,000$ – $5,000^\circ/\text{s}^2$), for which the VOR normally dominates gaze stabilization. Each stimulus was repeated 10 times, and sets of stimuli were delivered in random order for each experiment. During each pulse train period, the recording room was entirely dark to ensure the monkey's VOR was not suppressed by visual input. However, 50 ms after the beginning of the 500-ms rest period that occurred between pulse trains, an LED was illuminated directly in front of the monkey's face to recenter the monkey's gaze and then turned off 50 ms before the next pulse train.

Pulse rate and current modulation without baseline stimulation

With no baseline stimulation rate (BSR) and no baseline stimulation current (BSC) delivered to the labyrinth, we recorded eye movement responses to pulse trains of various pulse rates and current amplitudes. The range of tested current amplitudes (which varied by SCC) was divided into seven current levels (CL), where CL7 was the maximum current (above which facial nerve stimulation was evident), CL2 was threshold current (below which significant

eye movements were not evoked), CL1 was a sub-threshold current (equal to $CL2 - 0.2 \times (CL7 - CL2)$), and CL3 through CL6 were evenly distributed current amplitudes between CL2 and CL7. The range of tested pulse rates was from 100 to 600 pps (steps of 100 pps). A total of 36 unique stimulus pulse trains were delivered for each SCC, comprising all possible combinations of six current steps (CL2–CL7) and six pulse rate steps.

Pulse rate and current modulation with baseline stimulation

After measuring eye movement responses to stimuli without any baseline stimulation, we examined responses after adaptation to baseline stimulation, which is necessary for eliciting inhibitory eye responses. (The charge-balanced, biphasic, pulsatile stimuli delivered by the MVP2 are exclusively excitatory, so the only way to encode inhibition with a single MVP2 is to withdraw excitation.) The monkeys were adapted to one of two (BSR, BSC) combinations: (94 pps, CL4), and (200 pps, CL6). They were allowed to acclimate to this baseline stimulation in the light until their “spontaneous” nystagmus in darkness fell below 5 °/s (lights were turned off briefly once every 15 min to observe nystagmus, which was more pronounced in darkness). This typically took ~30 min when adapting to (94 pps, CL4), and ~4 h when adapting to (200 pps, CL6). Following this adaptation period, we recorded eye responses to steps in pulse rate at constant current amplitude (rate modulation up to 600 pps), steps in current amplitude at constant pulse rate (current modulation up to CL7), and steps in both rate and current simultaneously (co-modulation up to 600 pps, CL7, and down to 0 pps, CL1).

Alignment precompensation

Once we determined the effects of co-modulating stimuli above and below baseline stimulation, we used the alignment precompensation strategy (Fridman et al. 2010a) in conjunction with co-modulating stimuli to decrease response misalignment that resulted from electrode cross talk. To characterize the implanted animal’s VOR performance over a wide range of possible head movements, we sequentially stimulated the animal with 38 different sets of stimuli representing 38 head movements about unique axes of rotation. For each stimulus set, we used the 3-vector \vec{s} to represent the relative stimulus intensities that effectively encoded the three components of 3D angular velocity during a given head rotation. For example, if maximum stimulus intensity elicited a VOR of 125 °/s about the Z-axis with stimulation on

the left horizontal SCC electrode only, a VOR of 200 °/s about the left-anterior/right-posterior SCC plane (LARP) axis with stimulation on the left-anterior SCC electrode only, and a VOR of 180 °/s about the right-anterior/left-posterior SCC plane (RALP) axis with stimulation on the left-posterior SCC electrode only, the prosthesis could encode head velocities of 125, 200, and 180 °/s about the Z, LARP, and RALP axes, respectively, assuming a VOR gain of 1 (Dai et al. 2011b) and no electrode cross talk. If the head were rotated about an arbitrary axis (as detected by the MVP2’s gyroscopes) represented by $\vec{g} = [50 \text{ °/s}, 150 \text{ °/s}, 90 \text{ °/s}]$ where each element of \vec{g} represents the component of head rotation about the Z, LARP, and RALP axes, respectively, the appropriate stimulation intensity representing this head motion on the electrode targeting the horizontal SCC would be the ratio of the \vec{g} component about the Z-axis (50 °/s) divided by the maximum head velocity that could be encoded about the Z-axis (125 °/s), which equals 0.4. The same calculation would follow for the components of head rotation about the LARP and RALP axes, yielding $\vec{s} = [0.4, 0.75, 0.5]$. Thirty-eight unique \vec{s} vectors were selected to sample the range of all possible axes of eye rotations (Fig. 1). The direction of each vector represents the desired axis of eye rotation, and the length represents the magnitude of the desired eye velocity resulting from each \vec{s} . Primarily due to current spread and electrode cross talk, the recorded eye responses were often misaligned with the desired eye responses. We characterized this response misalignment by measuring the responses \vec{r}_i (a 3-vector representing the eye response velocity about the Z, LARP, and RALP axes) to 38 unique 3-vectors \vec{s}_i . We then calculated a 3×3 matrix M using least-squares techniques such that

$$\vec{r}_i \approx M \vec{s}_i \quad \text{for } i = 1 \dots 38 \quad (1)$$

This matrix M can be used to adjust the stimulus intensity on each electrode and compensate for misalignment effects due to cross talk. The appropriate pattern of compensated electrode stimulation intensity \vec{a} the prosthesis should deliver during a head rotation represented by \vec{g} is

$$\vec{a} = M^{-1} \vec{g} \quad (2)$$

We compared the magnitude and alignment of eye responses to all 38 \vec{s}_i vectors with and without alignment precompensation. All precompensation

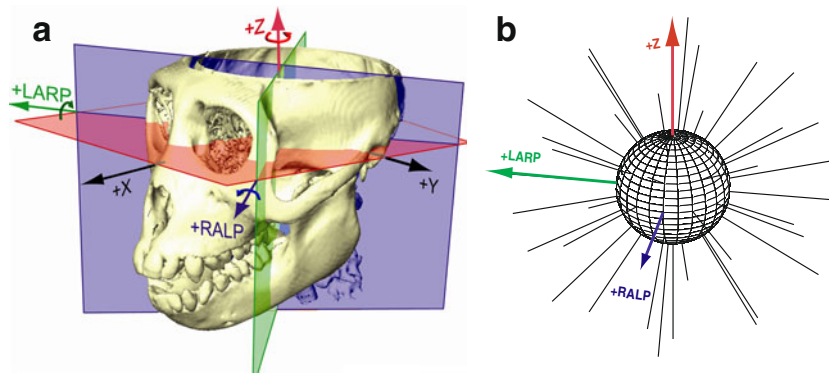


FIG. 1. **A** SCC coordinate system used for description of head rotation and 3D VOR eye rotation responses. $+X$, $+Y$, and $+Z$ vectors intersect at the stereotactic origin (i.e., the midpoint of the interaural axis) and are perpendicular to the stereotactic coronal, sagittal, and horizontal planes, respectively (Della Santina et al. 2005b). Left-anterior/right-posterior (+LARP), right-anterior/left-posterior (+RALP), and $+Z$ vectors represent the cardinal axes of the SCC coordinate system. Curved arrows depict the direction of positive rotation about each axis. **B** Thirty-eight unique vectors were selected to characterize the VOR responses to prosthetic stimulation. Each vector corresponds

to a unique head rotation and desired eye response movement and contains three elements representing the stimulus intensity on each electrode (targeting the horizontal, superior, and posterior canal ampullary nerves). The direction of each vector represents the desired axis of eye rotation, and the length represents the magnitude of the desired eye velocity resulting from each \vec{s} . Ideally, eye rotations exclusively about the Z , LARP, or RALP axes would be elicited by electrical stimulation of only the left horizontal, left-anterior, or left-posterior canal electrodes, respectively.

experiments were conducted following adaptation to high baseline stimulation (200 pps, CL6) to maximize inhibitory eye velocity.

Direction-specific alignment correction

We reasoned that excitatory and inhibitory stimuli may exhibit different levels of cross talk, and therefore, alignment precompensation may work best if tuned specifically for each head rotation axis. For example, when all three electrodes deliver excitatory stimuli, an eye response may have a different degree of misalignment as compared with an eye response to all three electrodes delivering inhibitory stimuli. To account for this, we divided up the 3D space of possible head rotation axes into eight octants, whose borders were the horizontal SCC plane (Z), LARP plane, and RALP plane. Instead of calculating one transformation matrix for all stimuli as before, we calculated an individual transformation matrix for each octant. The inverse of each matrix was then used to compute alignment precompensated stimulus commands for that matrix's octant, which were subsequently delivered to each monkey while we recorded eye movements. To address the issue of which transformation matrix to use when a desired vector was on a border between multiple octants, we created "virtual" octants whose borders were the misaligned Z , LARP, and RALP planes of rotations that were elicited in response to uncompensated stimuli. For example, when stimulating solely on the horizontal SCC electrode, the desired axis of rotation

would be the earth-vertical axis, which is at the intersection of four "ideal" octants. However, since elicited responses were not perfectly aligned with desired axes of rotation, "virtual" octants were different from "ideal" octants, and the earth-vertical axis fell inside one of the virtual octants instead of on the border between multiple octants. When a desired vector was within the boundaries of a "virtual" octant, the transformation matrix of that octant was used to correct the alignment of that vector. Therefore, the 38 vectors (Fig. 1) were distributed over the eight octants with some octants having fewer vectors and some having more vectors, depending on the location of the "virtual" octants. This allowed for each electrode to deliver exclusively excitatory or inhibitory stimuli throughout each "virtual" octant.

Following all recordings, we compared eye movement responses to all 38 stimulus vectors under three conditions: control (stimulation without any precompensation), precompensation with one transformation matrix, and precompensation with eight transformation matrices.

Eye movement analysis

Eye movement data were analyzed using a custom software package written in LabVIEW that incorporates 3D rotational kinematics (Migliaccio et al. 2005). The calculated SCC axes [based on $+X$ (nasal), $+Y$ (left), $+Z$ (superior, perpendicular to the mean horizontal SCC plane)] were the left-anterior/right-posterior axis (+LARP: $[x, y, z]=[1, -1, 0]/$

$\sqrt{2}$), the right-anterior/left-posterior axis (+RALP: $[x, y, z]=[1, 1, 0]/\sqrt{2}$), and the horizontal axis ($[x, y, z]=[0, 0, 1]$). For eye responses to transient stimuli, each of these three components was separately averaged cycle by cycle.

Eye rotation velocity components were calculated from 3D eye position data using rotational kinematic algorithms and linearly interpolated on a 1-kHz time base, filtered by a low-pass filter (50-order zero-phase finite impulse response filter at 40 Hz) and then smoothed by a running spline interpolation filter (LabVIEW “Cubic Spline Fit” module with balance parameter 0.999999). For each stimulus cycle, this procedure yielded three waveforms (describing the Z, LARP, and RALP components of eye angular velocity in SCC coordinates), each of which was then averaged across time (for 100 ms after each stimulus onset) on a cycle-by-cycle basis to create the mean cycle-averaged 3D eye velocity as a function of time after stimulus onset. To facilitate comparison of relative VOR performance across different stimulus paradigms, we extracted two values—peak eye velocity and misalignment—from mean cycle-averaged response traces.

Peak eye velocity was defined as the peak eye speed (i.e., magnitude of the 3D eye velocity vector) of a movement that began within the first 50 ms of stimulus onset, peaked within the first 100 ms of stimulus onset, and was in the direction appropriate for VOR slow-phase responses to the stimulus.

The angle of axis misalignment was computed as the angle between the peak eye velocity magnitude vector and the desired axis of rotation. Trials in which the monkey blinked or fell asleep were disregarded. Statistical analysis was performed using the MATLAB Statistics and Optimization packages (Mathworks, Natick, MA). Aggregate values are reported as mean \pm sample standard deviation (SD).

RESULTS

Excitatory responses to co-modulation

VOR-mediated eye velocity in the excitatory direction generally increased with both increasing pulse rate and increasing current amplitude for all three SCC electrodes tested in both monkeys when they were not previously adapted to baseline stimulation (Fig. 2). Simultaneously increasing both pulse rate and current amplitude (co-modulation) elicited significantly larger eye responses than either rate or current amplitude modulation elicited alone. The largest peak excitatory response velocity observed ranged from 419 to 854 $^{\circ}/s$ across different SCCs, which is

within the range of the majority of transient head velocities experienced by a person during typical daily activity (Grossman et al. 1988). The effects of pulse rate and current amplitude on misalignment of responses were not statistically significant (ANOVA: $p=0.68, 0.44$, respectively).

Slow-phase VOR responses to intense stimuli often exceeded 200 $^{\circ}/s$ and 1,000 $^{\circ}/s^2$. We distinguished these robust “slow-phase” eye movements from saccadic quick phases by noting that slow-phase response movements scaled with stimulation intensity and were in the direction appropriate for a VOR slow-phase response to the head rotation the stimulus was meant to represent. Spontaneous nystagmus in darkness (as a result of gentamicin treatment) was less than 5 $^{\circ}/s$ and at least 20 times smaller than typical electrically evoked eye velocities and, therefore, had a negligible effect on the observed trends. Additionally, this nystagmus was suppressed and not observed while the fixation LED was illuminated between stimulus pulse trains and only returned after 2 to 3 s in darkness. Therefore, it is unlikely that the nystagmus significantly contributed to the measured evoked eye movements that occurred within 100 ms of LED illumination.

Inhibitory responses following adaptation to higher baselines

To encode inhibitory head movements with a unilaterally implanted vestibular prosthesis constrained to deliver excitatory pulses, one must adapt the animal to nonzero baseline stimulation and then down-modulate the stimulus below this baseline. However, elevated baseline stimulation levels tend to come at the cost of decreased excitatory eye velocities (Lewis et al. 2010).

We explored responses to stimuli above and below two different baseline levels: (94 pps, CL4), and (200 pps, CL6). Immediately following baseline stimulation onset, peak excitatory eye velocities were observed ranging from 37 to 96 $^{\circ}/s$ (94 pps, CL4) and 77 to 364 $^{\circ}/s$ (200 pps, CL6) as seen in Figure 2. Following ~ 30 min (94 pps, CL4) or ~ 4 h (200 pps, CL6) of adaptation, nystagmus decreased to <5 $^{\circ}/s$.

Figure 3 shows examples of excitatory and inhibitory eye response traces (averages of 10 trials) to stimulation of the left horizontal SCC of monkey 1 following adaptation to either high or low baselines. These eye movements were in response to maximum stimulus intensity for each modulation type. Smaller eye velocities and accelerations not depicted here were elicited in response to lower stimulus intensities. When the monkey was adapted to a low baseline (94 pps, CL4), rate modulation elicited a significantly larger eye response (Fig. 3A) than when the monkey

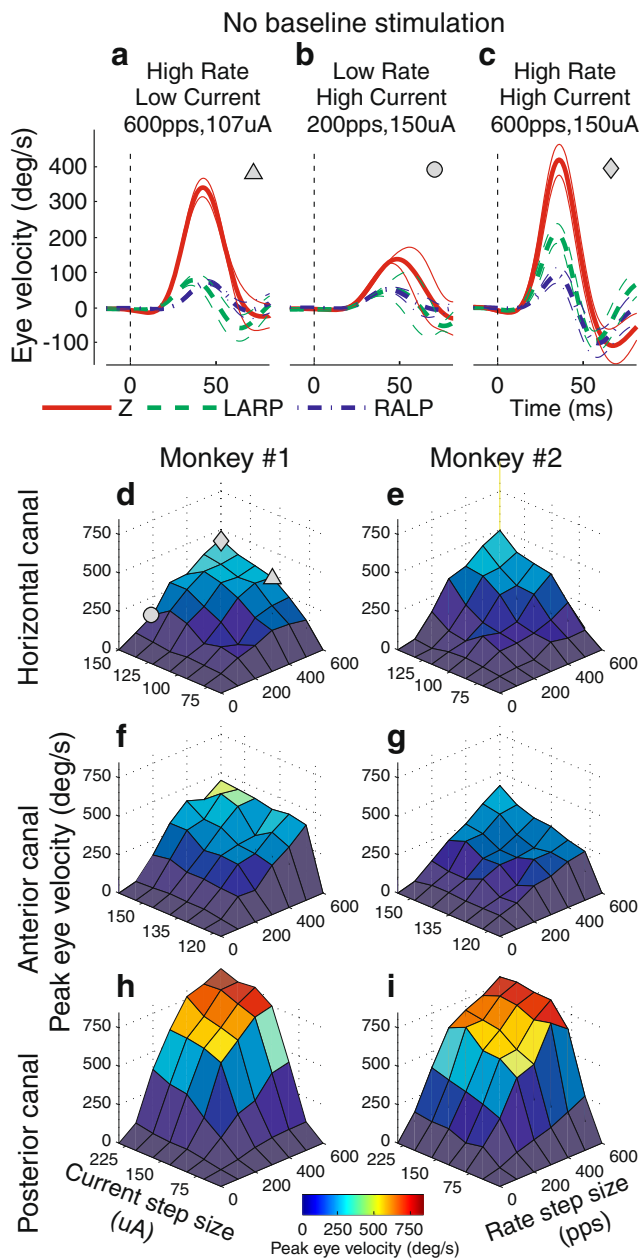


FIG. 2. A–C Examples of cycle-averaged eye movements for animal 1's left horizontal semicircular canal in response to stimulation steps from a zero baseline (0 pps, 0 μ A) to (600 pps, 107 μ A) (A), (200 pps, 150 μ A) (B), and (600 pps, 150 μ A) (C). All pulses were 150 μ s/phase, biphasic, symmetric, and charge balanced. Eye responses are displayed as mean (*thick trace*) \pm SD (*thin traces*) for eye rotational velocity components about Z (*red, solid trace*), LARP (*green, dashed trace*), or RALP (*blue, dot-dashed trace*) axes. *Dashed lines* indicate stimulus onset. **D–I** Surface plots of peak eye velocities of responses to 36 unique stimulation steps in pulse rate and pulse current amplitude from a zero baseline (0 pps, 0 μ A). Three of these responses are depicted in panels **A**, **B**, and **C** and correspond to the *triangle*, *circle*, and *diamond* in panel **D**, respectively. Peak eye response velocities increase with rate and with current amplitude. Responses are shown for all three tested semicircular canals for both tested monkeys.

was adapted to a high (200 pps, CL6) baseline (Fig. 3E). In contrast, current modulation elicited a slightly larger eye response following adaptation to (200 pps, CL6) (Fig. 3B, F). After adaptation to either baseline, co-modulation elicited a larger eye response than either rate or current modulation alone (Fig. 3C, G). Most importantly, the inhibitory eye response was significantly larger following adaptation to the higher baseline (Fig. 3D, H) even though excitatory response to co-modulation was smaller following adaptation to this higher baseline (Fig. 3C, G). Rate modulation down to 0 pps and current modulation down to 0 μ A are mathematically identical to co-modulation

down to 0 pps, 0 μ A, since no stimulation can be delivered when either the pulse rate or current amplitude is 0.

The same trends were observed when responses from all six tested SCCs were averaged together: excitatory responses to co-modulation were significantly smaller after adaptation to a high baseline, while inhibitory responses significantly increased (but were still relatively small compared to excitatory responses; Fig. 4). Even though adaptation to a higher baseline resulted in decreased excitatory responses, the increased inhibitory eye velocity of these movements yielded greater excitatory/inhibi-

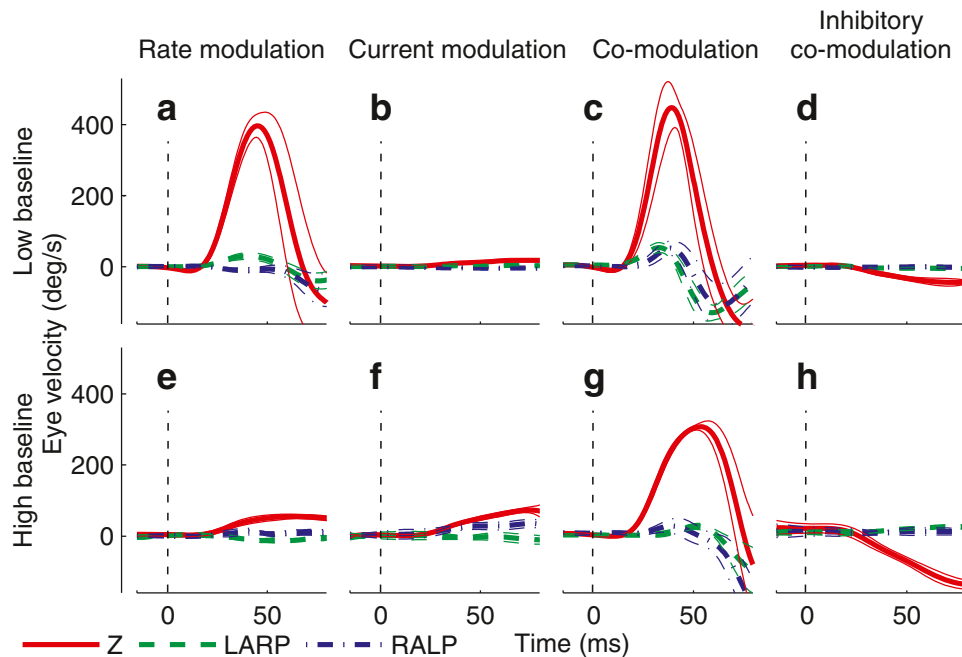


FIG. 3. Cycle-averaged eye response traces following adaptation of animal 1's left horizontal SCC ampullary nerve to baseline stimulation rate and current of 94 pps, 107 μA (A–D) or 200 pps, 121 μA (E–H). Eye responses are displayed as mean (*thick trace*) \pm SD (*thin traces*) for eye rotational velocity components about Z (*red, solid trace*), LARP (*green, dashed trace*), or RALP (*blue, dot-dashed trace*) axes. The *dashed line* indicates stimulus onset time. **A, E** Step in pulse rate to 600 pps (maximum delivered pulse rate) while current was held constant. **B, F** Step in current to 150 μA (maximum delivered current amplitude) while pulse rate was held constant. **C, G** Step in both pulse rate and current up to 600 pps, 150 μA . **D, H** Step in both pulse rate and current down to (0 pps, 0 μA). Rate modulation down to 0 pps and current modulation down to 0 μA are mathematically identical to co-modulation down to 0 pps, 0 μA , since no stimulation can be delivered when either the pulse rate or current amplitude is 0. Compared to either rate-only or current-only

modulation, co-modulation yielded largest excitatory and inhibitory eye movements regardless of baseline. Considering the goal of effectively encoding both excitatory and inhibitory head rotations, co-modulation from a high baseline yielded the best overall performance. Although responses to excitatory stimuli in this condition were less robust than observed for the low-baseline paradigm, responses for inhibitory stimuli (i.e., down-modulating both pulse rate and current amplitude from a high baseline) were more robust than those achieved with the low-baseline paradigm, with responses approaching $3,000\text{ }^\circ/\text{s}^2$. In some cases, stimulus duration and intensity were sufficient that the resulting slow-phase VOR eye movement drove the eye to near its range of motion limit shortly after modulation onset. As a result, the downward deflections seen in **A, C,** and **G** represent nystagmus quick phases.

tory response symmetry, which is crucial to restoring a VOR that can compensate for head movements in *all* directions.

Response alignment and magnitude with precompensation

Although stimulating SCC ampullary nerves with co-modulating stimuli following adaptation to a high baseline can elicit large eye responses in both excitatory and inhibitory directions, cross talk between stimulating electrodes often results in eye responses that are misaligned with their intended axis of rotation. We sought to correct this using an alignment precompensation strategy that we previously proved effective in chinchillas stimulated using a pulse–frequency–modulation encoding strategy (Fridman et al. 2010a). We compared the misalign-

ment and velocity magnitude values of all stimulus test vectors under three conditions: (1) control [i.e., all 38 vectors (Fig. 1) without any precompensation], (2) precompensated stimuli using one transformation matrix for all 38 vectors, and (3) precompensated stimuli using eight transformation matrices; one for each octant of the response sphere (Fig. 1). For all three conditions, the desired eye velocity was $81\text{ }^\circ/\text{s}$ for monkey 1 and $28\text{ }^\circ/\text{s}$ for monkey 2. Even though larger velocities could be elicited in most directions, we chose to limit the desired velocity of all stimuli to the response velocity elicited by the stimulus vector \vec{s}_i with the smallest response for each monkey. For both monkeys, inhibitory stimulation of the left-anterior (LA) SCC resulted in the smallest peak eye velocity response. Stimulation intensity on all other SCCs and directions in each monkey were scaled down to match the small eye velocity elicited by each LA SCC. In this

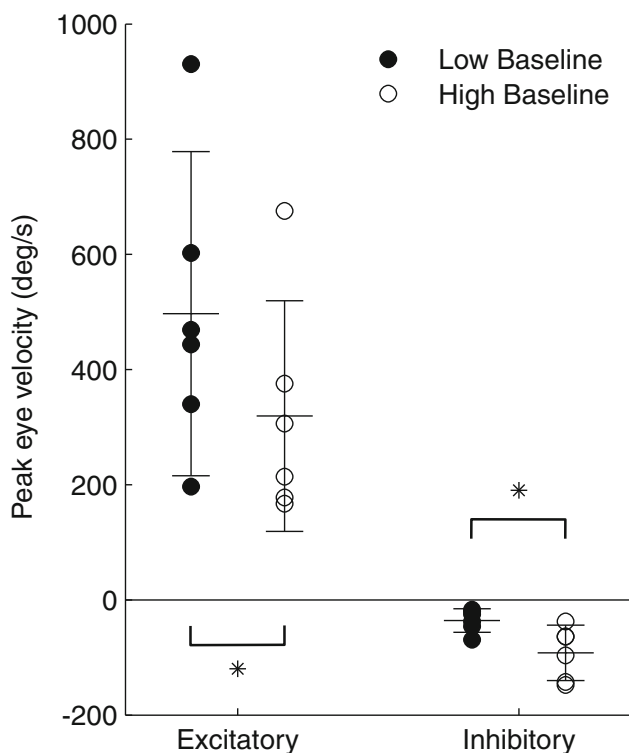


FIG. 4. Peak eye velocities from each of six tested SCCs in response to co-modulation above (excitatory) or below (inhibitory) either low or high baseline stimulation that the monkey was adapted to. The trends observed in Fig. 3 for one SCC were consistent for all six. At high baseline, excitatory velocity was smaller but inhibitory velocity was larger. * represents significant difference between two datasets at the $p < 0.01$ level (paired t test).

manner, we controlled for desired velocity by making it equal across all stimulation directions (as depicted by equal-magnitude vectors in Fig. 1), which would not have been possible if we had used stimulation vectors that elicited larger eye velocities in only certain directions. This allowed for more accurate comparison of each response's misalignment.

There was a significant effect of compensation type on mean misalignment and eye velocity for both monkeys ($p < 0.01$; repeated measures ANOVA). Post hoc paired t test analyses are described below that compare effects of individual conditions. When we delivered all stimulation vectors under the control condition, we observed mean misalignment of $21 \pm 13^\circ$ for monkey 1 and $26 \pm 16^\circ$ for monkey 2. For both monkeys, these mean misalignment values were not significantly different from those observed in response to precompensated stimuli with one transformation matrix, which were $23 \pm 15^\circ$ for monkey 1 and $21 \pm 8^\circ$ for monkey 2 ($p = 0.20, 0.78$, respectively; paired t test). However, eye responses to stimuli after precompensation with eight octant-specific transformation matrices resulted in mean misalignment of $14 \pm 10^\circ$ for monkey 1 and $17 \pm 10^\circ$ for monkey 2, both significantly better than mean misalignment values in response to control stimuli and precompensated stimuli with one matrix ($p < 0.012$; paired t test). In addition to improved misalignment, precompensated stimuli elicited more accurate eye velocities than uncompensated stimuli. Precompensated stimuli for monkey 1 elicited a mean eye response

velocity of $76 \pm 14^\circ/\text{s}$ with eight transformation matrices and $85 \pm 20^\circ/\text{s}$ with one matrix, while uncompensated stimuli elicited a mean velocity of $105 \pm 24^\circ/\text{s}$. Both types of precompensated responses were significantly closer to the desired velocity of $81^\circ/\text{s}$ and had smaller variance than did responses to uncompensated stimuli ($p < 0.01$; paired t test). Similar results were observed for monkey 2, which had a desired velocity of $28^\circ/\text{s}$ and mean response velocities of $29 \pm 8^\circ/\text{s}$ for eight matrices, $27 \pm 9^\circ/\text{s}$ for one matrix, and $44 \pm 19^\circ/\text{s}$ for uncompensated stimuli ($p < 0.01$; paired t test).

Six examples of uncompensated and precompensated (with eight matrices) averaged eye response traces are shown in Figure 5A and B. Panels C and D of Figure 5 show the 3D eye rotation axes measured with and without precompensation for each monkey. The stimulus vectors chosen in these figures were intended to elicit eye responses solely about the RALP, LARP, and Z rotation axes. Without precompensation, the eye responses already rotated about axes close to the intended axis of rotation. With precompensation, however, eye responses were even better aligned with their intended axes of rotation, and response velocities were closer to desired levels. For example, when the RALP axis was the intended axis of rotation for monkey 1 (Fig. 5A, lower panels), there was a significant response in both the RALP and the LARP planes without precompensation. In response to precompensated stimuli, the only significant response was in the desired RALP plane.

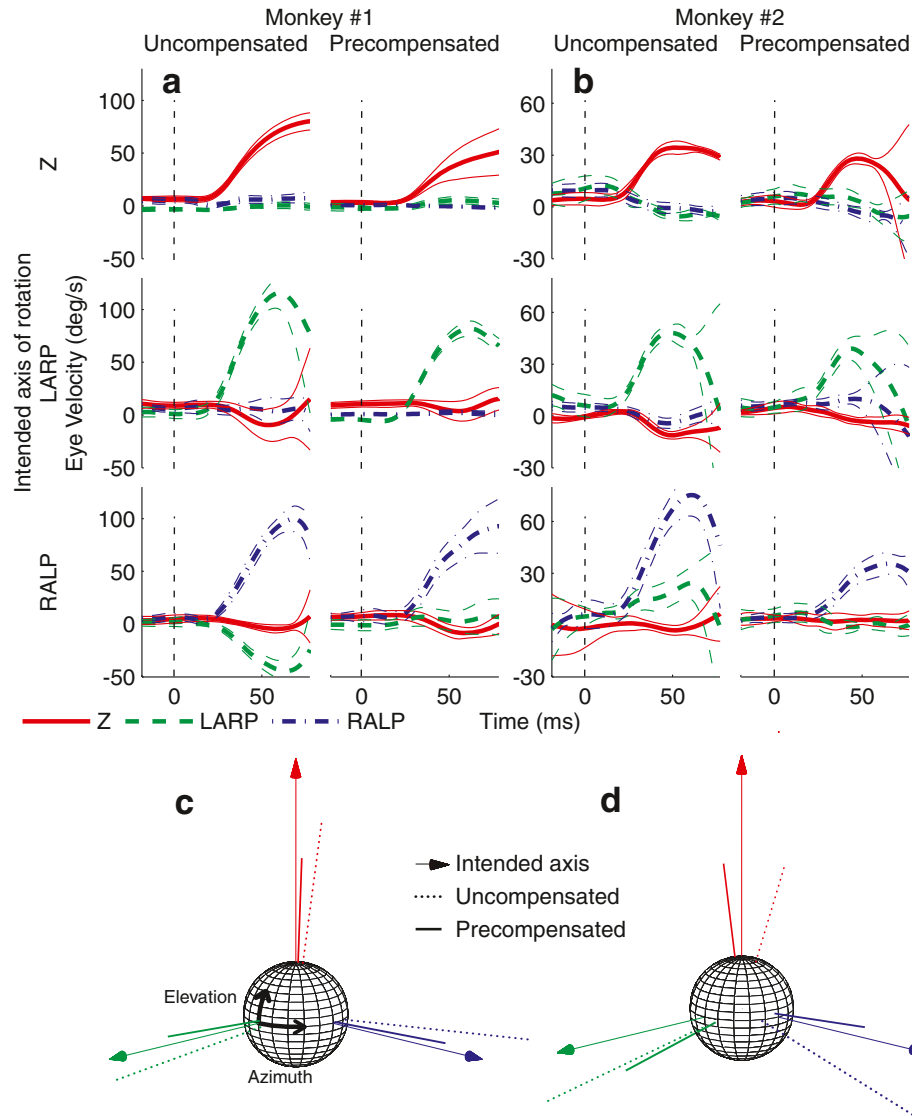


FIG. 5. A, B Cycle-averaged eye velocity traces for both monkeys with mean (*thick trace*) and SD (*thin traces*) in response to uncompensated and precompensated stimuli (with eight transformation matrices). The *dashed line* indicates stimulus onset time. The intended axis of rotation was Z, LARP, or RALP. In all cases, precompensated responses were better aligned than uncompensated responses to intended axis of rotation and closer to desired eye velocity (monkey 1, 81 %/s; monkey 2, 28 %/s). SD tended to be larger

near the latter portions of the response traces due to recovery quick phase eye movements that were more likely to occur at those times and were not synchronized with the stimulus onset. **C, D** Response vectors are depicted on a 3D sphere for easier visualization. The *thin arrow* represents intended axis of rotation, the *dashed line* represents uncompensated response vector, and the *solid line* represents precompensated response vector.

Figure 6 displays misalignment and eye velocity of responses to all 38 uncompensated and precompensated stimulus vectors (with eight matrices) for both monkeys. Projections of each data point's value on the left wall of each figure allow for easier visual comparison of responses across all directions. The dashed line on the left wall represents the ideal response in each case. As in the example above, precompensated responses had significantly less misalignment than uncompensated responses on average. Furthermore, in addition to being closer to the

desired eye velocity, eye velocity in response to precompensated stimuli had significantly less variance in comparison to uncompensated responses. For monkey 1, eye movements in response to uncompensated stimuli with an inhibitory RALP component tended to have particularly large misalignment values. For monkey 2, eye movements in response to uncompensated stimuli with an inhibitory Z component were poorly aligned. Alignment in both of these “problem regions” improved considerably in response to precompensated stimuli.

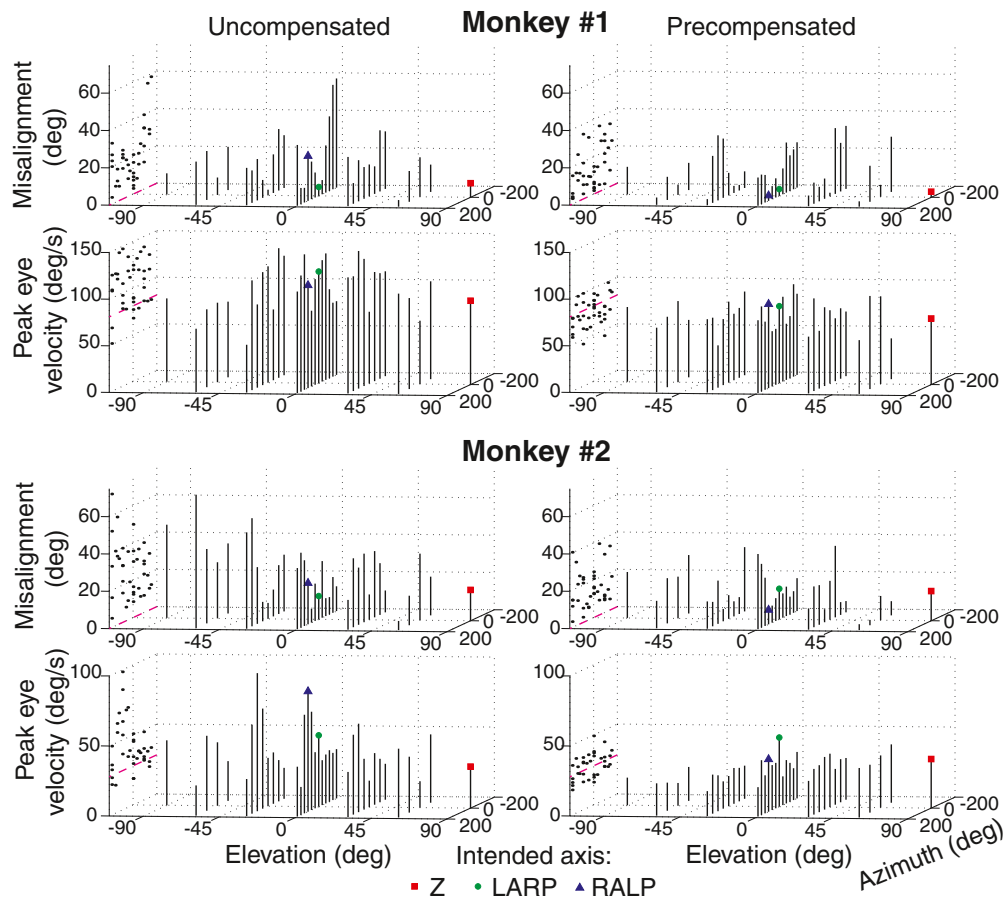


FIG. 6. Misalignment and eye velocity in response to all 38 uncompensated and precompensated (with eight transformation matrices) stimulation vectors for both monkeys. The X-axis represents azimuth (equivalent to longitude), and the Y-axis represents elevation (equivalent to latitude) on a theoretical sphere of possible eye rotations. Projections of each data point are depicted on the *left wall* of each panel for easier visual comparison. On average, misalign-

ment values were smaller, and eye velocities were closer to the desired velocity with less variance for responses to precompensated stimuli than for responses to uncompensated stimuli. *Dashed lines* represent desired misalignment (0° in all cases) or desired eye velocity. The *square*, *circle*, and *triangle* depict vectors with intended axes of Z, LARP, and RALP, respectively.

DISCUSSION

The primary goal of this study was to determine the most effective method for expanding the dynamic range of both excitatory and inhibitory eye movements in response to unilateral vestibular prosthetic stimulation while minimizing misalignment via alignment precompensation. We found that VOR eye responses to co-modulation were significantly larger than responses to rate or current modulation alone for all three baselines tested, and we found that inhibitory eye responses were largest when higher baselines were used. Alignment precompensation with eight direction-specific transformation matrices elicited eye responses with significantly less misalignment than with only one matrix or without any precompensation at all.

Effects of velocity encoding strategy on eye responses

Pulse rate modulation is an obvious choice for encoding head velocity with prosthetic vestibular stimulation, because it is most similar to spike rate encoding of the normal vestibular system. However, when a higher baseline is used (as is necessary to expand the dynamic range of responses to inhibitory head rotations), ceiling effects limit responses to excitatory stimuli encoded by pulse rate modulation alone (Fig. 3A, E). Simultaneous modulation of both rate and current amplitude gives an additional degree of freedom to encode head movements.

We observed that low pulse rate, high current, and high pulse rate, low current stimuli effectively evoked VOR eye responses of similar magnitudes, while co-modulating rate and current produced significantly

larger responses (Fig. 2). A possible explanation for this phenomenon (when observed in chinchillas) was offered by Davidovics et al. (2012). They suggested that increasing either current amplitude or pulse rate may increase the total number of action potentials (AP) firing on a vestibular afferent nerve since larger currents can increase the region of neural excitation, thereby recruiting more neural fibers to fire, and higher pulse rates can entrain a given population of nerve fibers to fire at higher frequencies (BeMent and Ranck 1969). Therefore, even though individual nerve fibers may fire at different rates in either condition, increasing the current or rate alone may increase the total number of APs produced on the entire vestibular afferent nerve branch. Since eye response velocities are similar in both conditions, it is possible that response velocity is proportional to the total number of spikes per second on the vestibular afferent nerve regardless of spike rates on individual nerve fibers. Recording of firing activity from individual nerve fibers would be necessary to determine if this purely speculative explanation is physiologically accurate. Electrical stimulation of muscle fibers and cortex demonstrates similar types of neural spatiotemporal summation (Kesar et al. 2008; Fridman et al. 2010b).

Adapting a monkey to sustained elevated spike rates appeared to dramatically limit the ability of a particular nerve branch to encode even moderate excitatory velocities. For the left horizontal SCC stimulation of monkey 1, rate modulation elicited a maximum eye velocity of 382 ± 43 °/s at (94 pps, CL4) (Fig. 3A) and 70 ± 9 °/s at 200 pps, CL6 (Fig. 3E). Even though rate modulation was not as effective at higher baselines, it is possible that the increased current with co-modulation may have been able to recruit “fresh” nerve fibers that had not been desensitized to electrical stimulation by adaptation and, therefore, still evoke large eye responses (Fig. 3H).

Effects of baseline stimulation on inhibitory eye responses

We evoked large inhibitory VOR eye velocities with unilateral prosthetic stimulation by adapting each monkey to artificially elevated baseline stimulation levels. Prior monkey vestibular prosthesis experiments typically adapted the animals to baseline stimulation rates of 94 pps (Dai et al. 2011b). However, inhibitory eye responses were only 36 ± 20 °/s when modulating below this baseline, and modulating below the higher baseline of (200 pps, CL6), elicited significantly larger inhibitory eye velocities of 92 ± 48 °/s ($p < 0.01$; paired *t* test, Fig. 4). Since large symmetric eye movements in all directions were desirable for alignment precompensation experiments, we adapted each monkey to the higher baseline before delivering those sets of

stimuli. The large variance observed between different SCCs for inhibitory eye velocity can likely be attributed to surgical variability in electrode placement, which influences the proximity of the electrode to the afferent nerve. The larger labyrinth size in humans will likely make it easier to accurately place each electrode and lead to more consistent responses between different SCCs.

Even though acceleration of eye responses in the inhibitory direction was significantly slower than acceleration in the excitatory direction (Fig. 3G, H), the inhibitory acceleration was $3,300 \pm 600$ °/s² in this case, which is larger than the great majority of typical head movements encountered in typical daily activities (Grossman et al. 1989).

Effects of alignment precompensation

Current spread is a problem inherent to electrical stimulation of the nervous system and often results in excitation of nontarget nerve fibers. A common solution is to use the smallest necessary stimulation current amplitude that achieves the desired response. With prosthetic vestibular stimulation, large currents are necessary to encode fast head rotations, which can lead to misaligned eye responses. Using the method of alignment precompensation, we were able to use large currents to elicit large eye responses that were relatively well aligned with their intended axis of rotation. It should be noted that these observed responses to precompensated stimuli were typically not as large as the electrical stimulation was capable of eliciting. This was because we chose to limit the desired velocity for all stimuli to the eye velocity elicited by the stimulus vector \vec{s}_i with the smallest response for each monkey so that misalignment could be accurately compared between responses. To account for electrode cross talk using the alignment precompensation method, each stimulus vector must be adjusted via a transformation matrix. This matrix was based on eye responses to nontransformed stimulus vectors. In general, if VOR axis of eye rotation is consistent for both excitatory and inhibitory responses for each SCC, then one transformation matrix should be sufficient to accurately transform stimulus vectors in any direction. However, if inhibitory responses have different axes of eye rotation than excitatory eye responses, a unique transformation matrix would be necessary to transform stimulus vectors in each case. Since there are three SCCs and each one can be stimulated in either the excitatory or inhibitory direction, there are eight unique combinations of SCC and direction of stimulation, resulting in the need for eight unique transformation matrices.

In contrast to our findings using a single precompensation matrix to improve the alignment of responses

in chinchillas (Fridman et al. 2010a), we did not observe improvement in alignment when using only one transformation matrix in monkeys. However, when using eight octant-specific matrices, we did observe significant improvements in alignment.

Differences between chinchillas and monkeys might have occurred for one of the following reasons. Firstly, monkeys had slightly better (although not significantly better due to small sample sizes) alignment than chinchillas on average before alignment precompensation [$24 \pm 4^\circ$ ($N=2$) vs. $28 \pm 14^\circ$ ($N=4$), $p=0.36$; t test], which was likely the result of better surgical placement of electrodes due to larger labyrinth size in monkeys. Since chinchillas had more room for improvement, alignment precompensation did not need to be as robust as compared to monkeys to produce significant improvement. Secondly, monkey eye movements were elicited using co-modulated stimuli, whereas chinchilla eye movements were elicited using rate-modulated stimuli. Since misalignment increases with increasing current (Della Santina et al. 2007; Davidovics et al. 2011, 2012), it is likely that responses to co-modulating stimuli (which have varying current amplitudes) of different intensities would have different degrees of misalignment. Significant differences in response misalignment between different octants would necessitate eight unique transformation matrices to significantly improve alignment.

Transitioning to human vestibular stimulation

While quantitative differences in optimal stimulation parameters between monkeys and humans are likely, general trends regarding effects of different stimulation strategies are probably conserved across species. Furthermore, because the separation between different vestibular nerve branches in the human labyrinth is ~ 1.45 times greater than in rhesus monkeys (Spoor and Zonneveld 1998), it is likely that humans would exhibit 3D VOR eye responses at least as close to normal as those observed in monkeys.

For human users of a vestibular prosthesis, adaptation time should be kept as short as possible, since the stimulus adaptation period may be uncomfortable for the user. In the present study, adaptation took ~ 4 h for monkeys exposed to high baseline stimuli. This duration may be shortened by exposing subjects to multiple on/off cycles (Merfeld et al. 2006; Lewis et al. 2010). Initial studies in humans suggest that they may adapt more quickly than do monkeys: Guyot et al. recently reported that a human receiving prosthetic vestibular stimulation adapted to a null in “spontaneous” nystagmus by ~ 27 min during the first off \rightarrow on cycle and in less than 5 min after several cycles (Guyot et al. 2011a).

Following adaptation to baseline stimulation, a human subject would undergo a fitting session in which a variety of stimulation test vectors would be presented (without the need for the subject to be physically moved) while the subject’s eye responses are measured using 3D oculography. We would then be able to characterize the uncompensated eye responses and program the prosthesis with appropriately calculated transformation matrices necessary to elicit well-aligned responses. As the subject adapts to prosthetic stimulation, it is likely that VOR alignment and magnitude will improve further as it did in chinchillas over a period of 7 days (Dai et al. 2011c). The stimulation strategies described in this paper, which were utilized to elicit large VOR responses in any desired direction in primates, provide a solid foundation for successful restoration of VOR in patients suffering from bilateral vestibular disorder.

ACKNOWLEDGMENTS

The authors thank Lani Swarthout for assistance with animal care. This research was supported by the US National Institutes of Health/National Institute on Deafness and Other Communication Disorders (NIH/NIDCD) grants R01DC009255, R01DC002390 and 1F31DC010099.

Conflict of interest

CCDS and GYF are inventors on university-assigned patents related to prosthesis technology. CCDS is the founder and CEO of Labyrinth Devices, LLC, in which he holds an equity interest. The terms of this arrangement are being managed by the Johns Hopkins University in accordance with its conflict of interest policies.

REFERENCES

- BE MENT SL, RANCK JB JR (1969) A quantitative study of electrical stimulation of central myelinated fibers. *Exp Neurol* 24:147–170
- BIERER SM, LING L, NIE K, FUCHS AF, KANEKO CRS, OXFORD T, NOWACK AL, SHEPHERD SJ, RUBINSTEIN JT, PHILLIPS JO (2012) Auditory outcomes following implantation and electrical stimulation of the semicircular canals. *Hear Res* 287:51–6
- BLACK FO, WADE SW, NASHNER LM (1996) What is the minimal vestibular function required for compensation? *Am J Otol* 17:401–409
- BLACK FO, GIANNA-POULIN C, PESZNECKER SC (2001) Recovery from vestibular ototoxicity. *Otol Neurotol* 22:662–671
- BLACK FO, PESZNECKER S, STALLINGS V (2004) Permanent gentamicin vestibulotoxicity. *Otol Neurotol* 25:559–569
- CAREY JP, MINOR LB, PENG GC, DELLA SANTINA CC, CREMER PD, HASLWANTER T (2002) Changes in the three-dimensional angular

- vestibulo-ocular reflex following intratympanic gentamicin for Ménière's disease. *JARO* 3(4):430–443
- CHIANG B, FRIDMAN GY, CHENKAI D, RAHMAN MA, DELLA SANTINA CC (2011) Design and performance of a multichannel vestibular prosthesis that restores semicircular canal sensation in rhesus monkey. *IEEE Trans Neural Systems Rehabil Eng* 19:588–598
- COHEN B, SUZUKI J, BENDER MB (1964) Eye movements from semicircular canal nerve stimulation in cat. *Ann Otol Rhinol Laryngol* 73:153–169
- CURTHOYS IS, HALMAGYI GM (1995) Vestibular compensation: a review of the oculomotor, neural, and clinical consequences of unilateral vestibular loss. *J Vestib Res* 5:67–107
- DAI C, FRIDMAN GY, DELLA SANTINA CC (2011A) Effects of vestibular prosthesis electrode implantation and stimulation on hearing in rhesus monkeys. *Hear Res* 277:204–210
- DAI C, FRIDMAN GY, DAVIDOVICS NS, CHIANG B, AHN JH, DELLA SANTINA CC (2011B) Restoration of 3D vestibular sensation in rhesus monkeys using a multichannel vestibular prosthesis. *Hear Res* 281:74–83
- DAI C, FRIDMAN GY, CHIANG B, DAVIDOVICS NS, MELVIN T, CULLEN KE, DELLA SANTINA CC (2011C) Cross-axis adaptation improves 3D vestibulo-ocular reflex alignment during chronic stimulation via a head-mounted multichannel vestibular prosthesis. *Exp Brain Res* 210:595–606
- DAVIDOVICS NS, FRIDMAN GY, DELLA SANTINA CC (2012) Co-modulation of stimulus rate and current from elevated baselines expands head motion encoding range of the vestibular prosthesis. *Exp Brain Res* 218:389–400
- DAVIDOVICS NS, FRIDMAN GY, CHIANG B, DELLA SANTINA CC (2011) Effects of biphasic current pulse frequency, amplitude, duration, and interphase gap on eye movement responses to prosthetic electrical stimulation of the vestibular nerve. *IEEE Trans Neural Systems Rehabil Eng* 19:84–94
- DELLA SANTINA C, MIGLIACCIO A, PATEL A (2005A) Electrical stimulation to restore vestibular function development of a 3-d vestibular prosthesis. *Conf Proc IEEE Eng Med Biol Soc* 7:7380–7385
- DELLA SANTINA CC, MIGLIACCIO AA, PATEL AH (2007) A multichannel semicircular canal neural prosthesis using electrical stimulation to restore 3-D vestibular sensation. *IEEE Trans Biomed Eng* 54:1016–1030
- DELLA SANTINA CC, POTYAGAYLO V, MIGLIACCIO AA, MINOR LB, CAREY JP (2005B) Orientation of human semicircular canals measured by three-dimensional multiplanar CT reconstruction. *J Assoc Res Otolaryngol* 6:191–206
- FRIDMAN G, DAVIDOVICS N, DAI C, MIGLIACCIO A, DELLA SANTINA C (2010A) Vestibulo-ocular reflex responses to a multichannel vestibular prosthesis incorporating a 3D coordinate transformation for correction of misalignment. *J Assoc Res Otolaryngol* 11:367–381
- FRIDMAN GY, BLAIR HT, BLAISDELL AP, JUDY JW (2010B) A quantitative model for the perceived intensity of cortical electrical stimulation. *Exp Brain Res* 203:499–515
- GONG WS, MERFELD DM (2000) Prototype neural semicircular canal prosthesis using patterned electrical stimulation. *Ann Biomed Eng* 28:572–581
- GONG WS, MERFELD DM (2002) System design and performance of a unilateral horizontal semicircular canal prosthesis. *IEEE Trans Biomed Eng* 49:175–181
- GONG WS, HABURCAKOVA C, MERFELD DM (2008) Vestibulo-ocular responses evoked via bilateral electrical stimulation of the lateral semicircular canals. *IEEE Trans Biomed Eng* 55:2608–2619
- GROSSMAN GE, LEIGH RJ, ABEL LA, LANSKA DJ, THURSTON SE (1988) Frequency and velocity of rotational head perturbations during locomotion. *Exp Brain Res* 70:470–476
- GROSSMAN GE, LEIGH RJ, BRUCE EN, HUEBNER WP, LANSKA DJ (1989) Performance of the human vestibuloocular reflex during locomotion. *J Neurophysiol* 62:264–272
- GUYOT J-P, GAY A, IZABEL KOS M, PELIZZONE M (2012) Ethical, anatomical and physiological issues in developing vestibular implants for human use. *J Vestib Res* 22:3–9
- GUYOT JP, SIGRIST A, PELIZZONE M, KOS MI (2011A) Adaptation to steady-state electrical stimulation of the vestibular system in humans. *Ann Otol Rhinol Laryngol* 120:143–149
- GUYOT JP, SIGRIST A, PELIZZONE M, FEIGL GC, KOS MI (2011B) Eye movements in response to electrical stimulation of the lateral and superior ampullary nerves. *Ann Otol Rhinol Laryngol* 120:81
- HASLWANTER T (1995) Mathematics of three-dimensional eye rotations. *Vis Res* 35:1727–1739
- HEPP K (1990) On Listing's law. *Commun Math Phys* 132:285–292
- HIRVONEN TP, MINOR LB, HULLAR TE, CAREY JP (2005) Effects of intratympanic gentamicin on vestibular afferents and hair cells in the chinchilla. *J Neurophysiol* 93:643–655
- KESAR T, CHOU L-W, BINDER-MACLEOD SA (2008) Effects of stimulation frequency versus pulse duration modulation on muscle fatigue. *J Electromyogr Kinesiol* 18:662–671
- LEWIS R, HABURCAKOVA C, GONG W, MAKARY C, MERFELD D (2010) Vestibuloocular reflex adaptation investigated with chronic motion-modulated electrical stimulation of semicircular canal afferents. *J Neurophysiol* 103:1066–1079
- LEWIS RF, MERFELD DM, GONG WS (2001) Cross-axis vestibular adaptation produced by patterned electrical stimulation. *Neurology* 56:A18–A18
- LEWIS RF, GONG WS, RAMSEY M, MINOR L, BOYLE R, MERFELD DM (2002) Vestibular adaptation studied with a prosthetic semicircular canal. *J Vestib Res-Equilib Orientat* 12:87–94
- LYFORD-PIKE S, VOGELHEIM C, CHU E, DELLA SANTINA CC, CAREY JP (2007) Gentamicin is primarily localized in vestibular type I hair cells after intratympanic administration. *J Assoc Res Otolaryngol* 8:497–508
- MAMOTO Y, YAMAMOTO K, IMAI T, TAMURA M, KUBO T (2002) Three-dimensional analysis of human locomotion in normal subjects and patients with vestibular deficiency. *Acta OtoLaryngol* 122:495–500
- MERFELD DM, HABURCAKOVA C, GONG W, LEWIS RF (2007) Chronic vestibulo-ocular reflexes evoked by a vestibular prosthesis. *IEEE Trans Biomed Eng* 54:1005–1015
- MERFELD DM, GONG WS, MORRISSEY J, SAGINAW M, HABURCAKOVA C, LEWIS RF (2006) Acclimation to chronic constant-rate peripheral stimulation provided by a vestibular prosthesis. *IEEE Trans Biomed Eng* 53:2362–2372
- MIGLIACCIO AA, TODD MJ (1999) Real-time rotation vectors. *Australas Phys Eng Sci Med* 22:73–80
- MIGLIACCIO AA, DELLA SANTINA CC, CAREY JP, NIPARKO JK, MINOR LB (2005) The vestibulo-ocular reflex response to head impulses rarely decreases after cochlear implantation. *Otol Neurotol* 26:655–660
- MIGLIACCIO AA, SCHUBERT MC, JIRAJEJVONG P, LASKER DM, CLENDANIEL RA, MINOR LB (2004) The three-dimensional vestibulo-ocular reflex evoked by high-acceleration rotations in the squirrel monkey. *Exp Brain Res* 159:433–446
- MINOR LB (1998) Gentamicin-induced bilateral vestibular hypofunction. *J Am Med Assoc* 279:541–544
- MINOR LB, LASKER DM, BACKOUS DD, HULLAR TE (1999) Horizontal vestibuloocular reflex evoked by high-acceleration rotations in the squirrel monkey I. Normal responses. *J Neurophysiol* 82:1254–1270
- NGUYEN KD, MINOR LB, DELLA SANTINA CC, CAREY JP (2009) Vestibular uncton and vertigo control after intratympanic gentamicin for Meniere's Disease. *Audiol Neurotol* 14:361–372
- NIE K, BIERER SM, LING L, OXFORD T, RUBINSTEIN JT, PHILLIPS JO (2011) Characterization of the electrically-evoked compound action potential of the vestibular nerve. *Otol Neurotol* 32:88

- RAMPRAHAD F, LANDOLT JP, MONEY KE, LAUFER J (1984) Dimensional analysis and dynamic response characterization of mammalian peripheral vestibular structures. *Am J Anat* 169:295–313
- RINNE T, BRONSTEIN AM, RUDGE P, GRESTY MA, LUXON LM (1998) Bilateral loss of vestibular function: clinical findings in 53 patients. *J Neurol* 245:314–321
- ROBINSON DA (1963) A method of measuring eye movement using a scleral search coil in a magnetic field. *IEEE Trans Biomed Eng* BM10:137–248
- RUBINSTEIN JT, BIERER S, KANEKO C, LING L, NIE K, OXFORD T, NEWLANDS S, SANTOS F, RISI F, ABBAS PJ (2012) Implantation of the semicircular canals with preservation of hearing and rotational sensitivity: a vestibular neurostimulator suitable for clinical research. *Otol Neurotol* 33:789–796
- SADEGHI SG, MINOR LB, CULLEN KE (2007) Response of vestibular-nerve afferents to active and passive rotations under normal conditions and after unilateral labyrinthectomy. *J Neurophysiol* 97:1503–1514
- SPOOR F, ZONNEVELD F (1998) Comparative review of the human bony labyrinth. *Am J Phys Anthropol Suppl* 27:211–251
- STRAUMANN D (1995) The validity of oculomotor laws. *Schweiz Arch Neurol Psychiatr* 146:151–156
- SUN DQ, RAHMAN MA, FRIDMAN G, CHENKAI D, CHIANG B, DELLA SANTINA CC (2011) Chronic stimulation of the semicircular canals using a multichannel vestibular prosthesis: effects on locomotion and angular vestibulo-ocular reflex in chinchillas. In: *EMBC, Annual International Conference of the IEEE*, pp 3519–3523
- SUZUKI J, COHEN B, BENDER MB (1964) Compensatory eye movements induced by vertical semicircular canal stimulation. *Exp Neurol* 9:137–160
- SUZUKI JI, COHEN B (1964) Head eye body and limb movements from semicircular canal nerves. *Exp Neurol* 10:393–405
- SUZUKI JI, GOTO K, TOKUMASU K, COHEN B (1969) Implantation of electrodes near individual vestibular nerve branches in mammals. *Ann Otol Rhinol Laryngol* 78:815–826
- TWEED D, VILIS T (1990) Geometric relations of eye position and velocity vectors during saccades. *Vis Res* 30:111–127
- WALL C, KOS MI, GUYOT JP (2007) Eye movements in response to electric stimulation of the human posterior ampullary nerve. *Ann Otol Rhinol Laryngol* 116:369–374